Molecular Neurobiology
https://doi.org/10.1007/s12035-018-1326-z

Suppressing Tau Aggregation and Toxicity by an Anti-Aggregant Tau Fragment

Ghulam Jeelani Pir[1,2] · Bikash Choudhary[1,2] · Senthilvelrajan Kaniyappan[1,2] · Ram Reddy Chandupatla[1,2] · Eckhard Mandelkow[1,2,3] · Eva-Maria Mandelkow[1,2,3] · Yipeng Wang[1,2]

Received: 14 June 2018 / Accepted: 20 August 2018
© The Author(s) 2018, corrected publication September/2018

Abstract

Tau aggregation is a hallmark of a group of neurodegenerative diseases termed Tauopathies. Reduction of aggregation-prone Tau has emerged as a promising therapeutic approach. Here, we show that an anti-aggregant Tau fragment ($F3^{\Delta KPP}$, residues 258–360) harboring the ΔK280 mutation and two proline substitutions ($I^{277}P$ & $I^{308}P$) in the repeat domain can inhibit aggregation of Tau constructs in vitro, in cultured cells and in vivo in a *Caenorhabditis elegans* model of Tau aggregation. The Tau fragment reduced Tau-dependent cytotoxicity in a N2a cell model, suppressed the Tau-mediated neuronal dysfunction and ameliorated the defective locomotion in *C. elegans*. In vitro the fragment competes with full-length Tau for polyanionic aggregation inducers and thus inhibits Tau aggregation. Our combined in vitro and in vivo results suggest that the anti-aggregant Tau fragment may potentially be used to address the consequences of Tau aggregation in Tauopathies.

Keywords Aggregation · Alzheimer disease · β-breaker peptides · Cell model · Microtubules · Tau · Transgenic *C.elegans* · Life-span

Introduction

The aggregation of the microtubule-associated protein Tau is a hallmark of Alzheimer disease and a number of other neurodegenerative diseases collectively termed Tauopathies. The nature of the Tau species (monomers vs. oligomers vs. fibers) that are the real culprits remains a matter of debate, but the process of Tau aggregation is generally linked to neurodegeneration [1, 2]. Thus, suppressing Tau levels and Tau aggregation has emerged as a promising therapeutic approach for treatment of Tauopathies [3, 4].

Tau is a natively unfolded protein, which exhibits very little tendency for aggregation on its own. Despite the fact that Tau can be induced to aggregate in vitro with the aid of polyanions, the trigger for Tau aggregation in vivo still remains unclear. Nevertheless, it is known that the aggregation of Tau is regulated by two hexapeptide motifs with enhanced β-propensity (^{275}VQIINK^{280} and ^{306}VQIVYK^{311}) in the second and third repeat of Tau [5]. Some Tau mutations in frontotemporal dementia (FTD) (e.g., ΔK280 & P301L) enhance β-propensity of the two hexapeptides and accordingly promote Tau aggregation[6]. By contrast, disruption of β-propensity via introducing two proline residues, known as β-structure breakers, into these hexapeptides (VQPINK & VQPVYK) prevents Tau aggregation and its toxicity [7]. Given their critical role in aggregation, the two hexapeptides become targets for developing inhibitors of Tau aggregation. Indeed, based on the structure of the two hexapeptides, a computer-aided design successfully identified several peptides showing high affinity to the

Bikash Choudhary and Senthilvelrajan Kaniyappan contributed equally to this work.

Electronic supplementary material The online version of this article (https://doi.org/10.1007/s12035-018-1326-z) contains supplementary material, which is available to authorized users.

✉ Ghulam Jeelani Pir
Jeelani.Pir@dzne.de

✉ Eva-Maria Mandelkow
Eva.Mandelkow@dzne.de

✉ Yipeng Wang
yipeng810@qq.com

[1] German Center for Neurodegenerative Diseases (DZNE), Sigmund-Freud-Str. 27, 53127 Bonn, Germany

[2] Max-Planck-Institute for Metabolism Research, Hamburg Outstation, c/o DESY, Notkestrasse 85, 22607 Hamburg, Germany

[3] CAESAR Research Center, Ludwig-Erhard-Allee 2, 53175 Bonn, Germany

Published online: 08 September 2018

two motifs, which inhibit Tau aggregation and thereby manifest therapeutic potential [8]. Similarly the inhibition of aggregation of other amyloidogenic proteins, such as Aβ, α-synuclein and prion protein can be achieved using β-sheet breaker peptides, i.e., peptides that are homologous to the targeted proteins but contain proline residues that interrupt the β-sheet structure [9, 10]. Although the introduction of proline into the hexapeptides can prevent self-aggregation of Tau in vitro and in vivo, it is not clear whether such β-breaker peptides of Tau can act as inhibitors of Tau aggregation and toxicity in cell and animal models.

Peptide-based therapy has been under consideration for some time; however, the nature of peptides—rapid degradation by proteases, low permeability across biological barriers (e.g., blood-brain barrier (BBB)) are intrinsic weaknesses that retard its therapeutic applications [11]. Nonetheless, recent years have seen a renaissance in gene therapy owing to the development of new technologies, e.g., genome editing tools (e.g., CRISPR-Cas9), and safer viral carriers (e.g., adeno-associated virus (AAV) and lentivirus) for delivery of genes into targeted cells (AAV) [12]. Our previous studies showed that the expression of anti-aggregant Tau in cultured cells or in transgenic mice does not cause overt side effects [13–15]. Thus in this study, we test whether a β-sheet breaker Tau fragment can inhibit Tau aggregation and thereby be potentially used for therapies for AD and other Tauopathies.

Materials and Methods

Cell Culture, Transfection and Treatments

The inducible Tet-On mouse neuroblastoma cell line (N2a) was generated as previously described [13]. The cells were cultured in Eagle's minimum essential medium (MEM) supplemented with 10% fetal bovine serum (FBS), 0.1% nonessential amino acids, and 600 μg/ml G418. The expression of Tau was induced with 1 μg/ml doxycycline. Transfection of N2a cells were performed with lipofectamine 2000 (Invitrogen) according to the manufacturer's manual. Twenty-four hours later, the conditioned medium was removed, and the cells were washed with warm PBS and then incubated in culture medium supplemented with 1 μg/ml doxycycline for 2 days to induce Tau expression.

Protein Preparation

Full-length Tau construct hTau40, Tau^{RD} construct (also known as K18, residues 244–372, comprising the four-repeat domain of Tau) harboring an FTDP-17 mutation ΔK280 ($Tau^{RD\Delta K}$) and its fragment $F3^{\Delta KPP}$ (residues 258–360, harboring ΔK280 with I^{177} and I^{308} in the two hexapeptide motifs at the second and third repeat domain of

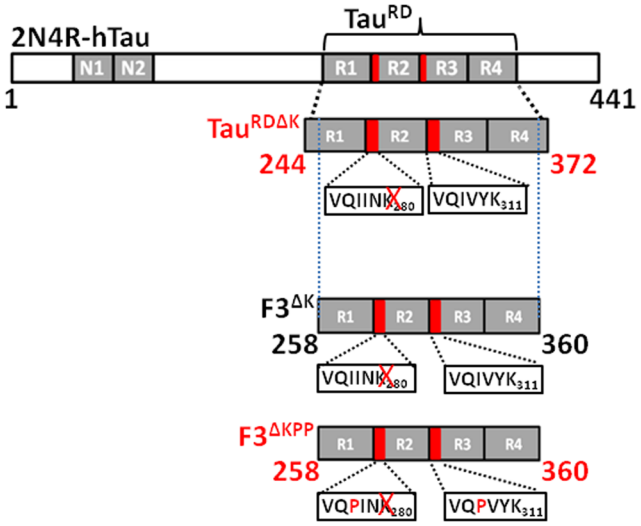

Fig. 1 Constructs of Tau. The top bar diagram represents the longest isoform of the human Tau40 (441 residues). The diagram below hTau40 shows the four-repeat construct Tau^{RD}. The two hexapeptides ($_{275}$VQIINK$_{280}$ and $_{306}$VQIVYK$_{311}$) are the motifs with the highest β-propensity at the beginning of the 2nd and 3rd repeat domains. The construct $Tau^{RD\Delta K}$ contains the FTDP-17 mutation ΔK280 that accelerates aggregation by promoting the β-structure (pro-aggregant mutant). The construct $F3^{\Delta K}$ is a proteolytic Tau fragment composed of aa. 258–360 [17, 18]. The construct $F3^{\Delta K\text{-}PP}$ harbors ΔK280 and has two proline mutations (I277P and I308P in the hexapeptide motifs) that inhibit aggregation by disrupting the β-structure (anti-aggregant mutant)

Tau mutated to proline) were prepared as described previously [16, 17] (Fig. 1). Tau constructs were obtained in expression vector pNG2 (a derivative of pET-3a (Merck-Novagen), employing site-directed mutagenesis using the QuickChange site-directed mutagenesis method (Stratagene). Recombinant proteins were expressed in the *Escherichia coli* BL21 (DE3) strain (Merck-Novagen). The expressed proteins were purified from bacterial extracts by using the heat stability of Tau protein and by FPLC SP-Sepharose (GE Healthcare). The cell pellet was resuspended in extraction buffer (50 mM MES, 500 mM NaCl, 1 mM $MgSO_4$, 1 mM EGTA, and 5 mM DTT, pH 6.8) supplemented with a protease inhibitor mixture (Roche Applied Science). The cells were disrupted with a French pressure cell and subsequently boiled for 20 min. The extracts were isolated by centrifugation, and the supernatant was dialyzed against cation exchange chromatography buffer A (20 mM MES, 50 mM NaCl, 1 mM $MgSO_4$,1 mM EGTA, 2 mM DTT, and 0.1 mM PMSF, pH 6.8) for two times and loaded on a FPLC SP-Sepharose column. The protein was eluted with a linear gradient of cation exchange chromatography buffer B (20 mM MES, 1 M NaCl, 1 mM $MgSO_4$, 1 mM EGTA, 2 mM DTT, and 0.1 mM PMSF, pH 6.8). The purity of proteins was ascertained by SDS-PAGE. Where necessary, breakdown products were removed by using the additional gel filtration column Superdex G75 with PBS buffer (137 mM NaCl, 3 mM KCl, 10 mM Na_2HPO4, 2 mM KH_2PO4, and 1 mM DTT, pH 7.4).

ThS Fluorescence

$Tau^{RD\Delta K}$ protein was dissolved at a concentration of 10 μM in PBS buffer supplemented with 2.5 μM heparin (Sigma, H3393, > 180 USP/mg, ~ MW 16 K), 1 mM dithiothreitol (DTT) and 40 μM thioflavine S (ThS). Different concentrations of F3ΔKPP (0, 10, 20, 40, and 80 μM) were mixed to the reaction mixture and the Kinetics of ThS fluorescence measured in a Tecan spectrofluorometer with an excitation wavelength of 440 nm and an emission wavelength of 521 nm (slit width, 2.5 nm each) in a black 384-well microtiter plate with round wells (Thermo Labsystems) using Magellan software. Measurements were carried out at 37 °C, and the background fluorescence was subtracted from respective blanks.

Pelleting Assay

The aggregated samples were centrifuged at 61000 rpm (100,000×*g*; TLA.100.3 rotor) to generate pellet fraction of aggregated Tau protein. The pellet was resuspended in the same volume as supernatant. The samples were run on a 17% SDS-PAGE gel and the amount of Tau protein in the supernatants and pellets were quantified by densitometry of the Coomassie Brilliant Blue R-250 stained gels using ImageJ analysis software.

Atomic Force Microscopy

One to two micromolar of Tau protein (after 24 h of $Tau^{RD\Delta K}$ aggregation (10 μM)) was diluted in PBS and placed on freshly cleaved mica for 10 min. The excess unbound protein was washed with PBS three times and the mica was filled with imaging buffer (10 mM Tris-HCl, pH 7.4, 50 mM KCl). AFM imaging was performed in oscillation mode using a Nano Wizard Ultra-speed AFM microscope (JPK instruments) and Si3N4 cantilevers (NPS series, Bruker) with spring constants of 0.1–0.6 N/m. Drive frequency of the cantilever tip was set using in-built auto-tune option. Surface approach was performed at 0.7 V. Later on, to achieve minimal imaging forces between AFM stylus and sample and also to compensate for the thermal drift of the AFM, the amplitude set point was adjusted manually. The acquired images were processed using JPK data processing software.

Electron Microscopy

Ten microliters of the samples (after performing the turbidity assay to monitor microtubule assembly) were incubated on glow discharged 200 mesh carbon-coated copper grids for 3 min followed by washing thrice with RB buffer and negatively stained with 2% filtered uranyl acetate for 30 s. Excess uranyl acetate was washed once with H_2O. The specimens were examined with a JEOL electron microscope at 200 kV at the electron imaging facility of CAESAR. Images of the microtubules were captured with a CCD camera using EMMENU 4 software.

Biochemical Assays

For solubility assays, cells were collected by centrifugation at 1000×*g* for 5 min. The levels and solubility of different Tau constructs were determined by sarkosyl extraction as previously described [17]. Supernatant and sarkosyl insoluble pellet samples were analyzed by Western blotting. The sarkosyl insoluble pellets and supernatants were loaded at 60:1 (pellet:supernatant). For quantification of Tau levels, the Western blots were probed with pan-Tau antibody K9JA (A-0024, DAKO, Glostrup, Denmark) and analyzed by densitometry.

Cytotoxicity Assays

Cytotoxicity was assessed by a LIVE-DEAD assay kit (Molecular Probes, Eugene, OR). For the LIVE-DEAD assay, N2a cells seeded on the coverslips were induced to express Tau constructs for 2 days. EthD (5 mM; Molecular Probes) was added to the medium to a final concentration of 2 μM and incubated at 37 °C for 30 min. Cells were fixed with 4% paraformaldehyde in PBS for 15 min and processed for immunofluorescence.

Immunofluorescence

Inducible N2a cells were either singly transfected with pBI5 plasmids encoding $Tau^{RD\Delta K}$ or $F3^{\Delta KPP}$ or co-transfected with these two plasmids. After 1 day, cells were induced to express Tau with 1 μg/ml doxycycline for 2 days. The cells on the coverslips were fixed with 4% paraformaldehyde in PBS for 15 min, then permeabilized with 0.1% triton at room temperature for 10 min, incubated with 0.1% ThS for 5 min, and washed three times in 50% ethanol. Samples were blocked in 5% BSA for 1 h at room temperature, followed by incubation with the primary and secondary antibodies. Confocal images were captured with a LSM700 microscope (Zeiss, Oberkochen, Germany).

Immunoprecipitation

Immunoprecipitation was done as described previously with slight modifications [17]. N2a cells were co-transfected with $Tau^{RD\Delta K}$-His and $F3^{\Delta KPP}$ or hTau40 and $F3^{\Delta KPP}$ and induced to express Tau for 2 days. Transfected N2a cells were rinsed twice with ice-cold PBS, lysed in homogenization buffer (50 mM Tris-Cl,

pH 7.4, 150 mM NaCl, 1% nonyl phenoxy polyethoxylethanol (NP-40), 10% glycerol, 1 mM ethylene glycol tetraacetic acid (EGTA), 20 mM NaF, 1 mM Na_3VO_4, 5 μM OA and protease inhibitor cocktail (Roche Applied Science,Basel, Switzerland) and incubated on ice for 30 min. After centrifugation at 16000×*g* at 4 °C for 20 min, the supernatant was collected and precleared with Dynabeads Protein G (Thermo Fisher Scientific; Dreieich, Germany) for 1 h at 4 °C. The lysates were incubated with control IgG or anti-His or DA9 antibodies overnight with constant rotation at 4 °C. Afterwards, Dynabeads Protein G was added to the lysates and incubated at 4 °C for 1 h. The beads were collected using a magnet and were washed four times with cold PBS, resuspended in Laemmli sample buffer, and analyzed by SDS-PAGE followed by Western blotting with Tau antibody K9JA.

For in vitro immunoprecipitation, recombinant proteins (50 μM hTau40, 200 μM $F3^{\Delta KPP}$ or a combination of both at 1:4 ratio) were incubated at 37 °C for at least 48 h in the presence or absence of 12.5 μM heparin (16 K). The reaction mixtures were incubated with control IgG or DA9 antibodies overnight with constant rotation at 4 °C in 1× Tris-buffered saline containing 0.05% Tween-20 Detergent (TBST). Afterwards, Dynabeads Protein G was added to the reaction mixtures and incubated at 4 °C for 3 h. The beads were collected using a magnet and were washed four times with cold 1× TBST, resuspended in Laemmli sample buffer, and analyzed by SDS-PAGE followed by western blotting with Tau antibody K9JA.

To detect the interaction between tau variants and heparin, recombinant proteins (50 μM hTau40, 200 μM $F3^{\Delta KPP}$ or a combination of both) were incubated at 37 °C for at least 48 h (or directly without incubation at 37 °C) in the presence or absence of 12.5 μM heparin (16 K). Afterwards, Dynabeads Protein G were added to the reaction mixtures directly without prior incubation with an antibody, and incubated at 4 °C for 3 h. The beads were collected using a magnet and washed four times with cold 1× TBST, resuspended in Laemmli sample buffer, and analyzed by SDS-PAGE followed by western blotting with Tau antibody K9JA.

Turbidity Assays

Tau-induced microtubule assembly was monitored by 90° angle light scattering at 350 nm in a Fluorolog spectrophotometer (HORIBA). Ten micromolar PC-purified tubulin were mixed with 5 μM Tau protein in RB buffer (100 mM PIPES, pH 6.9, 1 mM DTT, 1 mM $MgSO_4$, 1 mM EGTA, 1 mM GTP). Different concentrations of $F3^{\Delta KPP}$ (0, 5, 20, and 40 μM) were mixed to the reaction mixture and the polymerization started by transferring the ice-cold tubulin/Tau solution to the 37 °C warm cuvette holder at time point 0 min.

C. elegans Methods

Pan-neuronal *snb-1* promoter (gift of Dr. B.C. Kraemer, Seattle, WA) was used to drive the expression of cDNA construct encoding the $F3^{\Delta KPP}$ fragment. Transgenic arrays expressing $F3^{\Delta KPP}$ fragment were generated by injecting *Psnb-1::F3*$^{\Delta KPP}$ (50 ng/μl) plasmid along with the selection marker *Pofm::dsRed* (50 ng/μl) (gift of Dr. Naoki Hisamoto, Nagoya University) into the gonad of N2 wild-type strain (Bristol). Integration of transgene arrays into *C. elegans* genome was achieved by UV irradiation (300 J/m^2) and the resulting stable lines were out-crossed to N2 (Bristol) at least five times. Worm cultures were maintained according to the standard protocols [19]. Strains used were: PIR30: *pirIs30*[*Psnb-1::F3*$^{\Delta KPP}$*-low; Pofm::dsRed*], PIR31: *pirIs31*[*Psnb-1::F3*$^{\Delta KPP}$*-high; Pofm-2::dsRed*], CK10: *bkIs10*[*Paex-3::hTau1N4R* ^{V337M}*; Pmyo-2::gfp*] (gift of Dr. B.C. Kraemer, Seattle, WA), PIR32: *pirIs30;bkIs10*, PIR33: *pirIs31;bkIs10*, CZ1197: *juIs73*[*Punc-25::gfp*]III (gift of Dr. E. Lundquist, Lawrence, KS), PIR34: *pirIs32;juIs73*, PIR35: *pirIs32;juIs73*, *jsIs609:Is:*[*Pmec-4::MLS::gfp*] (gift of Dr. Nonet, St Louis, MO), PIR36: *pirIs32;jsIs609,* PIR37: *pirIs33;jsIs609*, PIR5: *psnb-1:: pirIs5*[*Psnb-1::hTau40A152T-low;Pmyo-2::gfp*], PIR38: *pirIs5;pirIs31.*

Behavioral Assay

The frequency of body bending (thrashes) was counted for 30 s after transferring the synchronized animals from each transgene in 20 μl of M9 buffer (22 mM KH_2PO_4, 42 mM Na_2HPO_4, 86 mM NaCl and 1 mM $MgSO_4$) on a glass slide and allowing them to settle for 1 min [20]. For micrographs, 1-day old worms were allowed to crawl for 10 min and photographed using an Olympus SZH10 fitted with SC30 camera.

Protein Extraction and Immunoblotting

For total worm lysates, 50 worms were dissolved in 30 μl 1× Laemmli buffer, boiled at 90 °C in a shaker for 10 min and loaded onto a 17% polyacrylamide gel for western blotting. To isolate the insoluble Tau, worm pellets were resuspended in high-salt RAB buffer [100 mM 2-(N-morpholino) ethanesulfonic acid (MES), 1 mM EGTA, 0.5 mM $MgSO_4$, 20 mM NaF] and lysed by sonication (6 × 10 s, 10 s break) on ice. Lysates were centrifuged at 40000×*g* for 40 min to yield the resulting supernatant as the soluble RAB fraction. The RAB pellet was suspended in RAB + 1 M sucrose buffer, centrifuged for 20 min at 40000×*g*, and the supernatant was discarded. The resulting pellet, after brief washing, was solubilized in urea containing buffer (UREA) [30 mM Tris, 7 M urea, 2 M thiourea, 4% CHAPS (3-[(3-cholamidopropyl) dimethylammonio]-1-propanesulfonate), pH 8.5]. All buffers

contained Complete Protease Inhibitor Mixture 3× (Sigma-Aldrich P8340, Hamburg, Germany), 1 μM Okadaic acid and 0.5 mM PMSF. Equal amounts of protein from each worm sample were loaded in separate gels, blotted and probed with antibodies against tau or the loading control tubulin. The following antibodies were used for immunoblotting: DM1α-tubulin (1:500; Sigma), K9JA (1:20,000; no. A0024; Dako), peroxide-conjugated secondary antibodies, and ECL solution (Thermo Scientific) were used to visualize the blots. AIDA software was used to perform densitometry.

Survival Assay

To prevent mixing of the generations, worms were transferred every second day to freshly seeded NGM plates until the fertility period was over. Survival assay was carried out at 20 °C and worms were scored every 1–2 days until death with L4 stage annotated as day 0. Animals were judged as dead if they did not respond to a gentle touch or push.

Imaging

Steady-state imaging of GFP-tagged mitochondria in mechanosensory neurons was performed by mounting worms on 2% agarose pads after anesthetizing in 50 mM sodium azide. Images were acquired at × 63 in two different regions, proximal part (~ 80 μm axonal part adjacent to cell body) and mid-region (beyond ~ 80 μm away from the cell body), using a Zeiss epifluorescence microscope equipped with a CCD (Photometrics) camera. To visualize the GABAergic motor neurons, young immobilized adults (15 mM sodium azide) were mounted on glass slides with 2% agarose pads and imaged at × 20 or × 40 using LSM 700 (Zeiss).

Results

β-Sheet Breaker Tau Fragment ($F3^{\Delta KPP}$) Reduces Tau Aggregation

Our previous study had shown that the overexpression of the repeat domain of Tau harboring an FTDP-17 mutation ΔK280 ($Tau^{RD\Delta K}$) in N2a cells results in the proteolytic generation of a fragment $F3^{\Delta K}$ (Fig. 1) [17]. We generated a β-sheet breaker Tau fragment via introduction of two prolines into the two hexapeptide motifs of $F3^{\Delta K}$, yielding $F3^{\Delta KPP}$ (Fig. 1). We tested whether recombinant $F3^{\Delta KPP}$ fragment can influence the aggregation of $Tau^{RD\Delta K}$ in vitro using thioflavine S (ThS) to monitor Tau aggregation. $F3^{\Delta KPP}$ alone does not form aggregates at all (black curve, Fig. 2a), which is consistent with our previous studies showing that the introduction of two β-breaking prolines into the two hexapeptides disrupts Tau aggregation. The aggregation of $Tau^{RD\Delta K}$ shows kinetics of nucleated assembly with an exponential phase followed by a plateau phase (red curve, Fig. 2a). $F3^{\Delta KPP}$ decreases the rate of $Tau^{RD\Delta K}$ aggregation in a concentration-dependent manner. At low concentrations (10 μM and 20 μM), the effect is small, and roughly similar plateau values are reached (olive and blue curves, Fig. 2a). In contrast, higher concentrations (40 μM and 80 μM, purple and green) of $F3^{\Delta KPP}$ noticeably decrease the assembly rate.

To further confirm that $F3^{\Delta KPP}$ treatment affects the aggregation of $Tau^{RD\Delta K}$, we separated soluble and insoluble Tau at the end of the incubation period via centrifugation and quantified their amounts by SDS-PAGE (Fig. 2b). When $Tau^{RD\Delta K}$ was incubated alone, ~ 60% of the protein formed aggregates (Fig. 2b, lane 2 and Fig. 2c, bar 1, red). In agreement with the results of the $Tau^{RD\Delta K}$ aggregation kinetic assay, addition of higher concentrations of $F3^{\Delta KPP}$ (40 μM and 80 μM) markedly reduces the aggregation of $Tau^{RD\Delta K}$, such that only 10% of $Tau^{RD\Delta K}$ appeared in the insoluble fraction (Fig. 2b, lanes 8 and 10 and Fig. 2c, bars 4,5, red). These results were corroborated by atomic force microscopy (AFM) analysis, which showed a reduction of fibrillar structures formed by $Tau^{RD\Delta K}$ in the presence of $F3^{\Delta KPP}$ (Fig. 2d, compare top and middle panel). As expected, $F3^{\Delta KPP}$ alone did not show any fibrillary structures (Fig. 2d, bottom panel).

$F3^{\Delta KPP}$ Reduces hTau40-Induced Microtubule Assembly

Being a microtubule-associated protein, Tau plays an important role in microtubule assembly. We therefore examined whether $F3^{\Delta KPP}$ interferes with this physiological function of Tau. Microtubule polymerization assays were performed with or without different concentrations of $F3^{\Delta KPP}$. Tubulin (at 10 μM) without Tau served as a negative control, as it is unable to self-assemble into microtubules below the critical concentration (Fig. 3, curve 1, green). Similarly, $F3^{\Delta KPP}$ alone is also unable to induce microtubule assembly (Fig.3, curve 2, olive). In the presence of full-length Tau (5 μM hTau40), tubulin polymerizes within about 8 min (Fig. 3, curve 5, red). At 1:1 concentration (5 μM hTau40 + 5 μM $F3^{\Delta KPP}$), microtubule assembly was slightly more efficient (Fig. 3, curve 6, black). However, at higher concentrations of $F3^{\Delta KPP}$, the rate and extent of polymerization decreased in a concentration-dependent manner (Fig. 3, curve 4, purple for 20 μM $F3^{\Delta KPP}$ and curve 3, blue for 40 μM $F3^{\Delta KPP}$). This was verified by electron microscopy (EM), which showed less microtubules that were often shorter and decorated with protein clumps when Tau (5 μM) and $F3^{\Delta KPP}$ (20 μM) was added (Fig. 3b, right image) compared to Tau alone (Fig. 3b, left image).

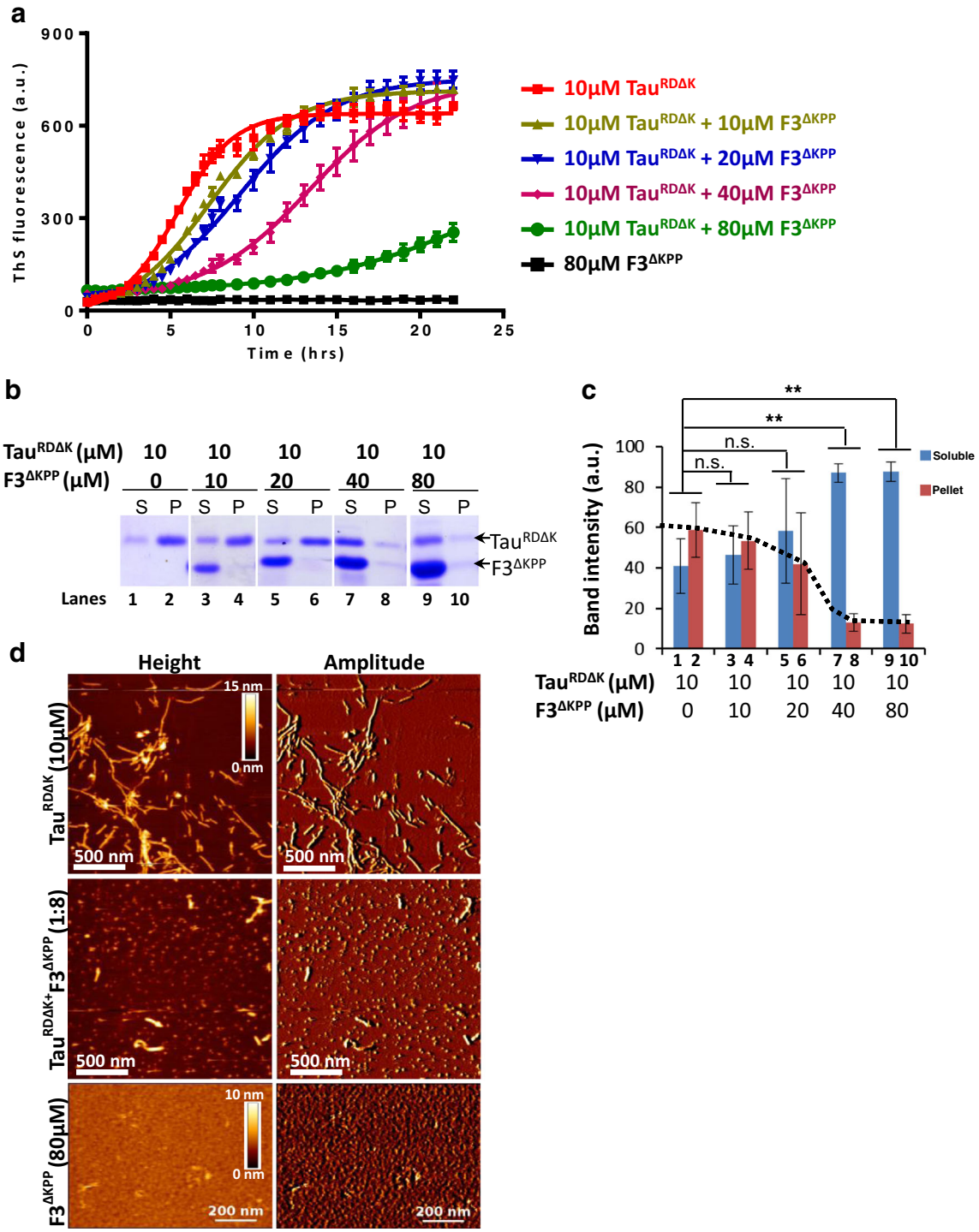

Fig. 2 $F3^{\Delta KPP}$ reduces $Tau^{RD\Delta K}$ aggregation in vitro. $Tau^{RD\Delta K}$ (10 μM, upper band) was induced to aggregate with heparin (2.5 μM) in the absence or presence of different concentrations of $F3^{\Delta KPP}$ (lower band) for up to 24 h. **a** The extent of aggregation as measured by the thioflavin S fluorescence assay. All the measurements were performed in triplicate, $n = 3$. **b** Pellet assay showing the distribution of soluble and aggregated $Tau^{RD\Delta K}$ (10 μM) alone (lanes 1, 2) or in the presence of $F3^{\Delta KPP}$ 10 μM (lanes 3, 4), 20 μM (lanes 5, 6), 40 μM (lanes 7, 8) and 80 μM (lanes 9, 10) at the end of incubation (S denotes the soluble fraction, P is the insoluble pellet fraction). **c** Densitometry quantification of the soluble (blue bars) and the insoluble (red bars) $Tau^{RD\Delta K}$ from the gel shown in (b). Note the suppression of $Tau^{RD\Delta K}$ aggregation at higher $F3^{\Delta KPP}$ concentrations (40 μM & 80 μM, red bars 8, 10). The results are from 3 different gels. One-way ANOVA was applied for multiple comparisons. Error bars denote SD. (ns, non-significant, $^{**}p < 0.001$). **d** In vitro aggregation of $Tau^{RD\Delta K}$ (10 μM) visualized using AFM in the absence (top panel) or presence (middle panel) of $F3^{\Delta KPP}$ (80 μM). 1–2 μM protein was diluted in PBS and placed on mica for imaging. No filamentous structures are seen in the presence of $F3^{\Delta KPP}$. $F3^{\Delta KPP}$ (80 μM) alone also does not form filamentous structures (bottom panel)

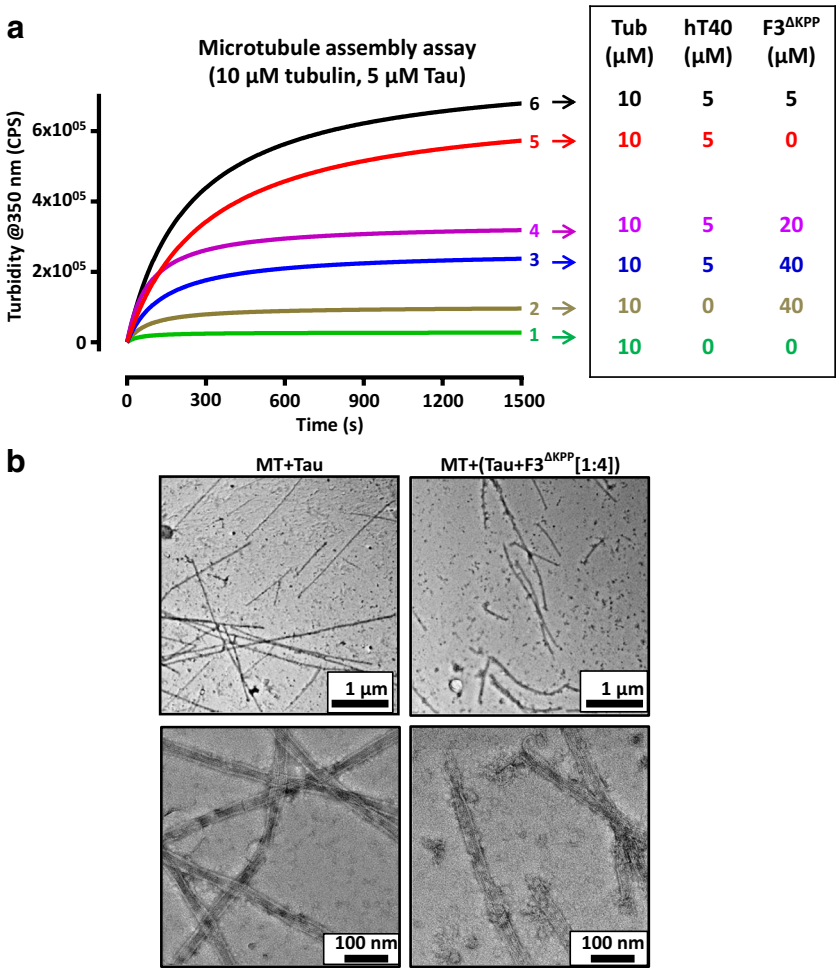

Fig. 3 $F3^{\Delta KPP}$ slightly reduces hTau40-induced microtubule assembly. Microtubule assembly was measured by light scattering at 350 nm in the absence or presence of hTau40 with or without different concentrations of $F3^{\Delta KPP}$. **a** Tubulin and hTau40 concentration was 10 µM and 5 µM respectively. The ratios between the concentration of hTau40 and $F3^{\Delta KPP}$ were 1:1, 1:4, and 1:8. Note that $F3^{\Delta KPP}$ reduces hTau40-induced microtubule assembly by ~ 50% (curves 4 and 3, purple and blue). Tubulin without Tau (curve 1, *green*) or with $F3^{\Delta KPP}$ alone (20 µM; curve 2, ochre) does not assemble in these conditions either. **b** Microtubule (10 µM) assembly induced by Tau (5 µM) visualized by negative stain electron microscopy in the absence (left panel) or presence (right panel) of $F3^{\Delta KPP}$ (20 µM). Microtubules are reduced with $F3^{\Delta KPP}$ and become more fragile

$F3^{\Delta KPP}$ Reduces Tau Aggregation and Cytotoxicity in a Cell Model of Tau Aggregation

Next, we examined whether $F3^{\Delta KPP}$ can inhibit Tau aggregation in cells. It is known that $Tau^{RD\Delta K}$ forms aggregates in N2a cells [17]. Therefore, we tested whether co-expression of $F3^{\Delta KPP}$ with $Tau^{RD\Delta K}$ influences the aggregation of $Tau^{RD\Delta K}$ in N2a cells. We used the ThS staining to visualize the Tau aggregates. When $Tau^{RD\Delta K}$ is expressed alone, ~ 20% of cells are positive for ThS (Fig. 4a, upper panel 1–3, Fig. 4b, bar 1). The co-expression of $F3^{\Delta KPP}$ reduces the ThS positive cells to ~ 9% (Fig. 4a, bottom panels 4–6, Fig. 4b, bar 2). We also evaluated Tau aggregation using sarkosyl extraction to separate soluble and insoluble Tau. Consistent with our previous studies [18], the expression of $Tau^{RD\Delta K}$ in cells results in its fragmentation (generating fragments $F2^{\Delta K}$, $F3^{\Delta K}$) which then nucleates Tau aggregation (Fig. 4c, lane 3). Notably, the co-expression of $F3^{\Delta KPP}$ inhibits the fragmentation of $Tau^{RD\Delta K}$ by cellular proteases, as no $F3^{\Delta K}$ fragment was observed in the pellet (Fig. 4c, lane 5). Accordingly, the aggregation is reduced in the presence of $F3^{\Delta KPP}$ (Fig. 4d, bar 2 in red).

Our previous studies have shown that the aggregation of Tau induces cell death in N2a cells [17, 21]. We therefore assessed whether $F3^{\Delta KPP}$ could rescue Tau aggregation-induced cell death. We monitored cell death via nuclear staining with EthD. When $Tau^{RD\Delta K}$ was expressed alone, 11% (11.1 ± 2.8%) of cells stained positive for EthD (Fig. 4e, upper panel 1–4, Fig. 4f, bar 1 in red). However, when $F3^{\Delta KPP}$ was co-expressed with $Tau^{RD\Delta K}$, only 4.5% (4.5 ± 2.6%) of cells showed EthD staining (Fig. 4e, bottom panel 5–8, Fig. 4f, bar 2 in gray). Moreover, consistent with our previous studies, the majority of the ThS positive cells were stained by EthD (Fig. 4e 1,2,4 and Fig. 4e 5,6,8), pointing to cytotoxicity induced by $Tau^{RD\Delta K}$ aggregation. Thus, $F3^{\Delta KPP}$ reduces $Tau^{RD\Delta K}$-induced cytotoxicity via inhibiting its aggregation.

$F3^{\Delta KPP}$ Suppresses Tau Pathology in an In Vivo *C. elegans* Model

Next, we turned to an in vivo model to test the protective efficacy of $F3^{\Delta KPP}$ fragment. We used the T^{VM} *C. elegans* model that expresses human 1N4R-Tau^{V337M} pan-neuronally

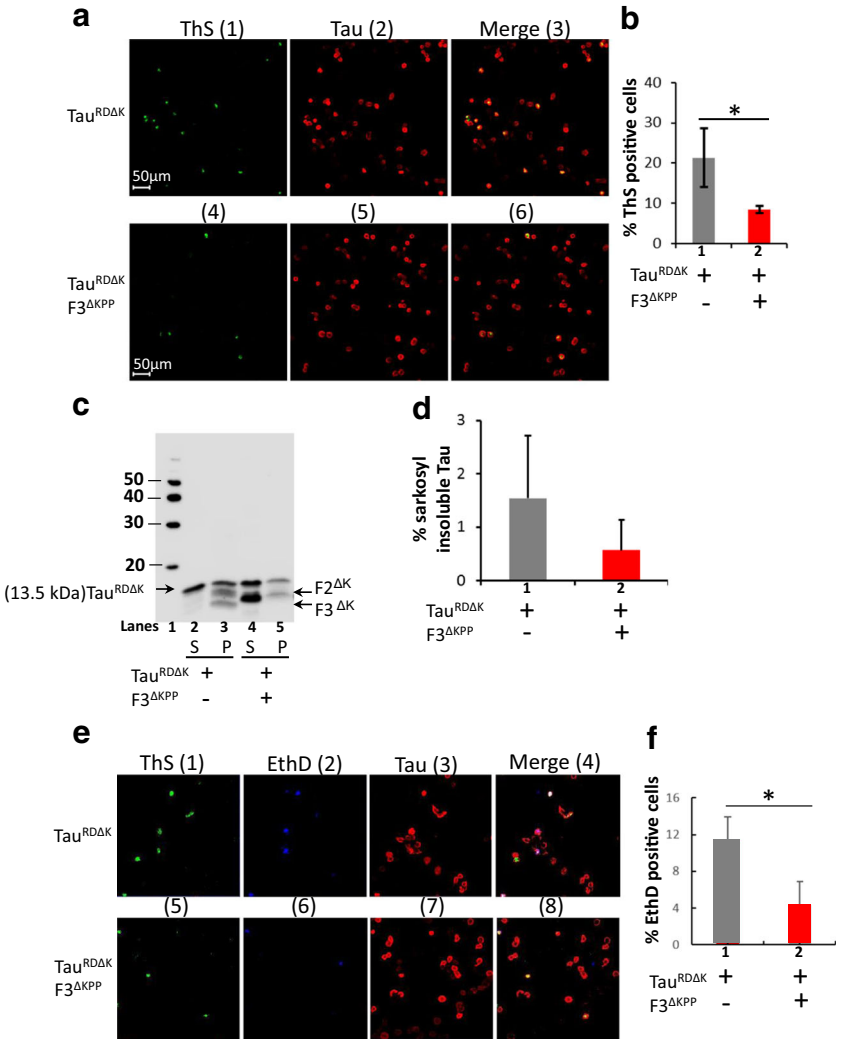

Fig. 4 $F3^{\Delta KPP}$ reduces $Tau^{RD\Delta K}$ aggregation and cytotoxicity in N2a cells. N2a cells were transfected with $Tau^{RD\Delta K}$ or co-transfected with $Tau^{RD\Delta K}$ and $F3^{\Delta KPP}$ for 2 days. **a** Thioflavin S (ThS) staining of Tau aggregates in N2a cells. Tau was monitored by immunostaining using a pan-Tau antibody K9JA (red panel 2 and 5). **b** Quantification of the ThS positive cells in relation to the Tau-expressing cells shown in (**a**). $F3^{\Delta KPP}$ strongly reduces ThS positive cells. (*t* test, $n = 3$; * $p < 0.05$). **c** Western blot analysis (17% PAGE, Tau antibody K9JA) of sarkosyl soluble (S) and insoluble (P) $Tau^{RD\Delta K}$ in the absence (lanes 2, 3) or presence (lanes 4, 5) of $F3^{\Delta KPP}$. **d** Densitometry quantification of insoluble $Tau^{RD\Delta K}$ (lanes 3 and 5) of the blot shown in (c). Note the strong reduction (~ 60%, red bar) of aggregated $Tau^{RD\Delta K}$ by co-expression of $F3^{\Delta KPP}$. (unpaired *t* test, $n = 6$; $p = 0.0624$). **e** Cell death monitored by nuclear staining with Ethidium Homodimer (EthD). Tau expression was determined by immunolabeling with antibody K9JA (panel 3 and 7), Tau aggregation by ThS staining (green), and cell death by EthD staining (blue). Note: that cell death (blue) was dramatically reduced by the co-expression of $F3^{\Delta KPP}$ (*t* test, SD, *$p < 0.05$). **f** Quantification of cells positive for EthD staining shown in E. Cell death was reduced by the co-expression of $F3^{\Delta KPP}$ (*t* test, SD, *$p < 0.05$)

[22]. This worm develops progressive motor dysfunction, neurodegeneration and accumulates detergent insoluble Tau aggregates. Since the protective effects of $F3^{\Delta KPP}$ were seen at higher stoichiometric ratios, we generated a transgenic *C. elegans* line $F3^{\Delta KPP}$-lo expressing $F3^{\Delta KPP}$ pan-neuronally at low levels, and another line $F3^{\Delta KPP}$-hi expressing $F3^{\Delta KPP}$ at higher levels. These lines were then individually crossed with T^{VM} resulting in double transgenic lines T^{VM};$F3^{\Delta KPP}$-lo and T^{VM};$F3^{\Delta KPP}$-hi. We first assessed total Tau levels in the parental T^{VM} worm and the double transgenic T^{VM};$F3^{\Delta KPP}$-lo and T^{VM};$F3^{\Delta KPP}$-hi worms, using the K9JA antibody which recognizes an epitope common to both the full-length Tau as well as the repeat fragment $F3^{\Delta KPP}$. Double transgenic T^{VM};$F3^{\Delta KPP}$-lo and T^{VM};$F3^{\Delta KPP}$-hi worms show comparable Tau levels as the single transgenic parental T^{VM} worm (Fig. 5a, lanes 2–4, Fig. 5b, bars 1–3).

T^{VM} worms show progressive motor dysfunction as seen by the distorted serpentine tracks left on the bacterial layer and lower thrashing rate when placed in liquid compared to non-transgenic control worms (compare Fig. 5c (1, 2) Fig. 5d, bars 1, 2). To check the protective effects of $F3^{\Delta KPP}$, we compared the motor function of these worms. $F3^{\Delta KPP}$ when co-expressed at higher levels in T^{VM};$F3^{\Delta KPP}$-hi results in improved motor function as seen by the near serpentine tracks

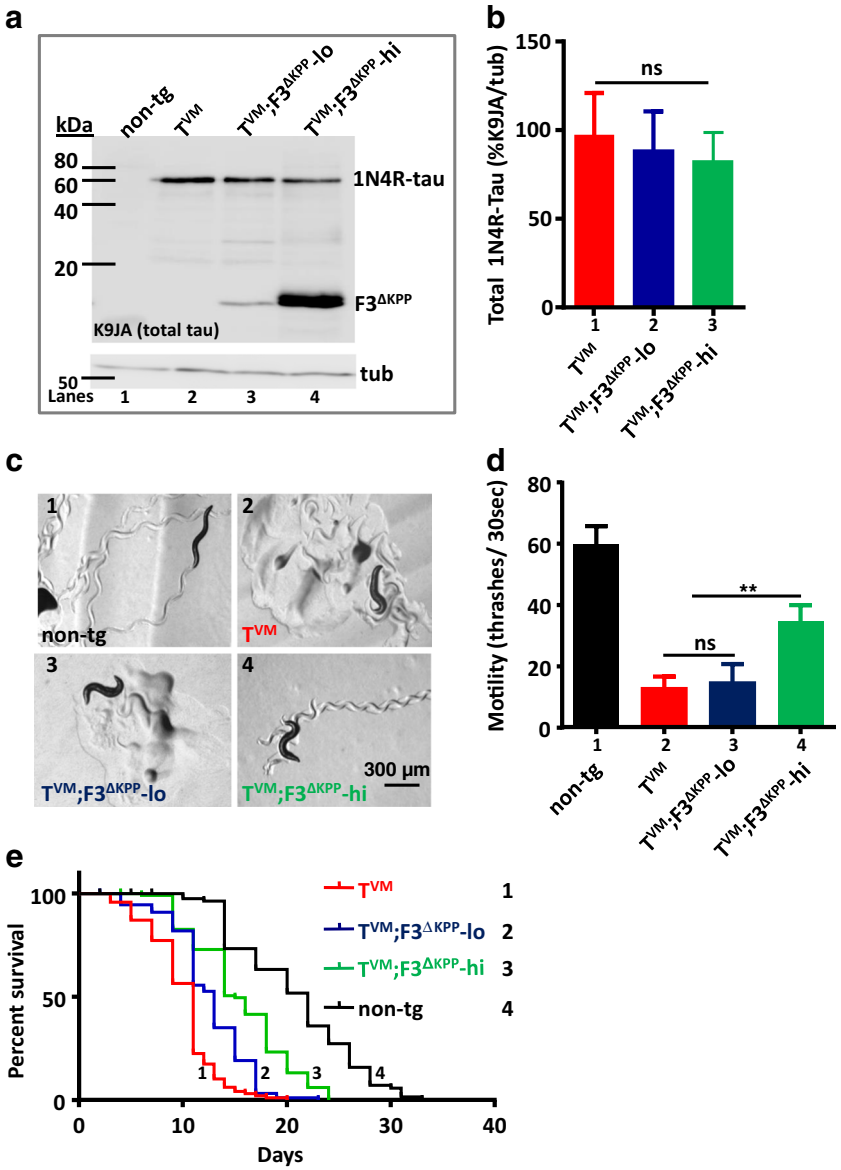

Fig. 5 $F3^{\Delta KPP}$ at higher levels ($F3^{\Delta KPP}$-hi) improves the motor deficits in a *C. elegans* Tau aggregation model (T^{VM}). $F3^{\Delta KPP}$ was expressed pan-neuronally in worms transgenic for human 1N4R-Tau^{V337M}. T^{VM} expresses human 1N4R-Tau^{V337M} pan neuronally. T^{VM};$F3^{\Delta KPP}$-lo and T^{VM};$F3^{\Delta KPP}$ -hi are doubly transgenic for human 1N4R-Tau^{V337M} and $F3^{\Delta KPP}$ at low and high levels respectively. **a** Western blot of the total worm lysates from synchronized 1-day-old adults using pan-Tau antibody K9JA. Tubulin served as internal control. **b** Quantification of the total Tau levels. One-way ANOVA with Tukey's test ($n = 3$, error bars denote SEM. ns, non-significant). **c** Micrographs showing tracks left behind by 1-day-old adults of the single and double transgenic worms. Non-transgenic (non-tg) served as control. **d** Body bending frequency (thrashes) of synchronized 1-day-old adults in liquid. Non-tg served as control, $n = 40$. One-way ANOVA with Tukey's test was applied for multiple comparisons. Error bars denote SEM. (ns, non-significant, $^{**}p < 0.01$). **e** Representative survival curves of single- T^{VM}, double- T^{VM};$F3^{\Delta KPP}$-lo, and T^{VM};$F3^{\Delta KPP}$-hi transgenic worms, non-tg served as control. Mantel-Cox log-rank test was performed to determine the statistical differences between genotypes

left by this worm and higher thrashing rate in liquid compared to the parental worm T^{VM} (Fig. 5c4, Fig. 5d, bar 4). However, T^{VM};$F3^{\Delta KPP}$-lo worm that co-expresses $F3^{\Delta KPP}$ at lower levels, failed to show any improvement in the motility (Fig. 5c3, Fig. 5d bar 3). T^{VM} worms show reduced survival such that T^{VM} worms live ~ 50% shorter compared to non-transgenic worms (Fig. 5e curve 1, red; curve 4, black). In combination with $F3^{\Delta KPP}$-hi, however, 20% increase in the median survival of the T^{VM} worm is observed (Fig. 5e curve 3, green; Table 1).

GABAergic motor neurons that coordinate the motor functions in worms show a compromised integrity in the parental T^{VM} worm [22]. These neurons can be visualized by using a reporter transgene *juIs73*:[*Punc-25::gfp*]III [23] that expresses GFP specific to this subset of neurons (Fig. 6a). Thus, T^{VM}, T^{VM};$F3^{\Delta KPP}$-lo, and T^{VM};$F3^{\Delta KPP}$-

Table 1 Statistical analysis of life-span assay performed as in Fig. 5e legend

Strain	Median survival	# deaths/total *N*	*p* value (vs non-tg)	*p* value (vs T^{VM})
Non-tg	22	70/120	–	$< 10^{-4}$
T^{VM}	11	100/120	$< 10^{-4}$	–
T^{VM};$F3^{\Delta KPP}$-lo	12	98/120	$< 10^{-4}$	$< 10^{-3}$
T^{VM};$F3^{\Delta KPP}$-hi	15	103/120	$< 10^{-4}$	$< 10^{-4}$

hi worms were crossed into this reporter strain to visualize the motor neurons in these worms. T^{VM} worms show significant neurodegeneration in the form of gaps in the dorsal and ventral nerve cords already at day 1 (~ 2 gaps) compared to non-tg reporter worms (~0.04 gaps). This does not differ from the T^{VM};$F3^{\Delta KPP}$-lo worms which also show a similar level of damage in these neurons (~ 1.96 gaps) (Fig. 6a (2, 3), Fig. 6b, bars 2,3). On the other hand, T^{VM};$F3^{\Delta KPP}$-hi worms with higher $F3^{\Delta KPP}$ levels show reduced neurodegeneration of the nerve cords (~ 1.08 gaps) (Fig. 6a4, Fig. 6b, bar 4). Thus an improvement in the integrity of motor neurons is consistent with an enhanced motility in T^{VM};$F3^{\Delta KPP}$-hi worms.

Since $F3^{\Delta KPP}$ inhibited Tau aggregation in vitro and in cell culture, we set out to investigate the status of insoluble Tau, a pathological hallmark of human Tauopathies that is also recapitulated by T^{VM} worms [22]. T^{VM} worms accumulate detergent insoluble Tau in their neurons. After extracting the soluble fraction, the insoluble Tau can be solubilized using a buffer with increasing solubilizing strength. Therefore, worm lysates from T^{VM}, T^{VM};$F3^{\Delta KPP}$-lo, and T^{VM};$F3^{\Delta KPP}$-hi were sequentially extracted by homogenizing the respective worm pellets first in a high salt containing RAB buffer, resulting in the soluble Tau fraction. The remaining Tau fraction, which corresponds to the insoluble Tau, was then isolated using urea buffer (see "Materials and Methods"). T^{VM};$F3^{\Delta KPP}$-hi worms

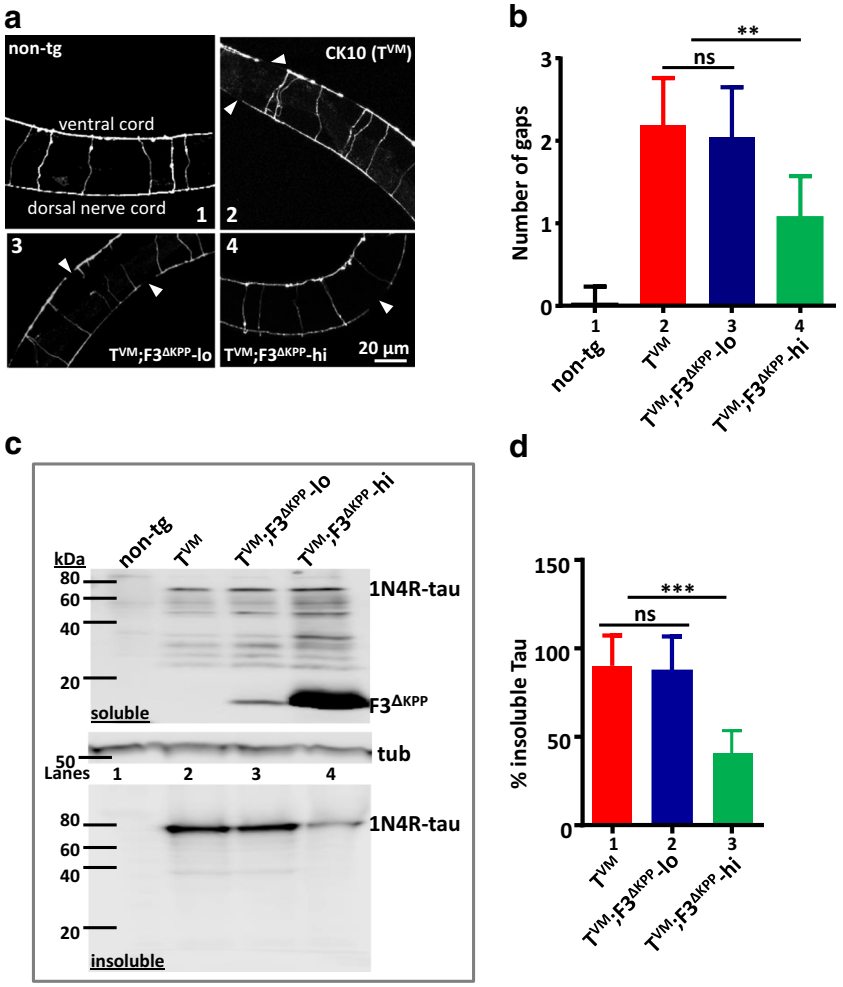

Fig. 6 $F3^{\Delta KPP}$-hi reduces morphological defects and suppresses the Tau aggregation in T^{VM}. **a** Fluorescence micrographs of GABAergic motor neurons in non-tg (1), T^{VM} (2), T^{VM};$F3^{\Delta KPP}$-lo (3), and T^{VM};$F3^{\Delta KPP}$-hi (4). Animals have ventral side oriented up. Arrowheads show gaps in the ventral and dorsal cord. **b** Number of gaps quantified in the neural cords of 1-day-old adults. Error bars denote SD. For comparison, one-way ANOVA with Tukey's test was applied ($n = 25$, ns, not significant, $^{**}P < 0.01$). **c** Sequentially extracted Tau from worm lysates of mixed stage animals resolved on 17% PAGE and immunoblotted using pan-Tau K9JA antibody. Tubulin served as a loading control. **d** Densitometry quantification of the insoluble Tau. T^{VM};$F3^{\Delta KPP}$-hi (insoluble panel, lane 4) shows reduced insoluble Tau (~ 50%). One-way ANOVA with Tukey's test ($n = 3$, error bars denote SEM. ns, non-significant, $^{***}P < 0.001$)

with higher $F3^{\Delta KPP}$ levels show a striking decrease in the detergent insoluble Tau aggregates compared to T^{VM} and T^{VM};$F3^{\Delta KPP}$-lo (Fig. 6c lower panel blot of insoluble protein, compare lane 4 with lanes 2, 3). Thus the fragment $F3^{\Delta KPP}$ shows protection by reducing the accumulation of insoluble Tau in T^{VM} worm neurons, in agreement with the results from in vitro and mammalian cell culture experiments described above.

Tau (both soluble monomeric and insoluble aggregates) is known to interfere with the axonal traffic in cell culture and animal models [24, 25] which leads to a disrupted localization of axonal cargoes. The fact that the insoluble Tau levels are reduced in T^{VM};$F3^{\Delta KPP}$-hi worms prompted us to look at the mitochondrial distribution. We generated mitochondrial reporter strains using *jsIs609* worms [24] that express GFP-labeled mitochondria in six mechanosensory neurons. We performed the static imaging of GFP puncta in proximal and mid-region of the mechanosensory neurons in all three worm lines in 1- and 3-day-old adults, using a non-tg reporter strain as control (see "Materials and Methods"). Schematics in Fig. 7a depict neurons with a normal and an abnormal mitochondrial distribution. The mitochondrial distribution in the parental T^{VM} worm neurons differs from those in the non-transgenic reporter worms at both time points, with fewer mitochondria in proximal and mid regions of axons. Notably, the distribution is much more affected in the mid regions of axons towards the distal end (Fig. 7b, c compare top- and mid-panel, Fig. 7d, e, bars 1–4). Furthermore, $F3^{\Delta KPP}$ co-expression improves the mitochondrial distribution towards the wild-type level. Thus, T^{VM};$F3^{\Delta KPP}$-hi (Fig. 7b c compare mid- and lower panel, Fig. 7d, e, bars 3–6) but not T^{VM};$F3^{\Delta KPP}$-lo (Sup Fig. 1A, B compare mid- and lower-panel, Sup Fig. 1C, D 3–6) worms show an increased number of mitochondria in both the proximal and the mid-regions of neurons. We conclude that a reduced insoluble Tau load in combination with an improved cargo localization in the T^{VM};$F3^{\Delta KPP}$-hi neurons improves the motility of these worms.

Peptide $F3^{\Delta KPP}$ Does Not Directly Interact with Other Tau Molecules in Cells

Previously we showed that the pro-aggregant fragment $F3^{\Delta K}$ can nucleate and promote the aggregation of full-length Tau when co-expressed in N2a cells. Using coimmunoprecipitation, we further demonstrated that this occurs as a result of direct interaction between the two Tau species [17]. Since $F3^{\Delta KPP}$ can inhibit $Tau^{RD\Delta K}$ aggregation, we asked whether this also results from a direct interaction with $Tau^{RD\Delta K}$. We tested this through an immunoprecipitation assay. Since there is no antibody that can differentially recognize $F3^{\Delta KPP}$ and $Tau^{RD\Delta K}$, we co-expressed $F3^{\Delta KPP}$ with $Tau^{RD\Delta K}$-His in N2a cells, and pulled down $Tau^{RD\Delta K}$-His with an antibody against the His tag. This pulled down $Tau^{RD\Delta K}$-His, but not $F3^{\Delta KPP}$

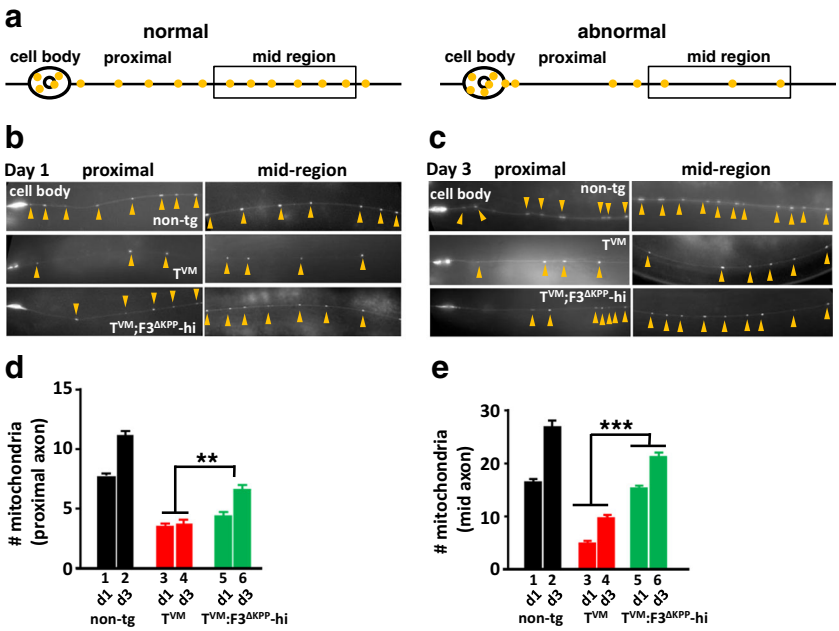

Fig. 7 $F3^{\Delta KPP}$-hi improves the mitochondrial distribution in *C. elegans*. **a** Schematic representation of neurons with a normal and abnormal mitochondrial distribution. **b** Representative images of GFP tagged mitochondria in the mechanosensory neurons of non-tg reporter strain, T^{VM} and T^{VM};$F3^{\Delta KPP}$-hi animals at day 1 of adulthood. **c** Representative images of GFP-tagged mitochondria in the mechanosensory neurons of non-tg reporter strain, T^{VM} and T^{VM};$F3^{\Delta KPP}$-hi animals at day 3 of adulthood. **d** Average number of mitochondria quantified in the proximal axon (~ 80 μm axonal part adjacent to cell body) at days 1 and 3. Student's *t*-test for comparison (error bars denote SEM. $^{**}P < 0.01$). **e** Average number of mitochondria quantified in the mid-region of the axon (beyond ~ 80-μm length from cell body) at days 1 and 3. Student's *t* test for comparison (error bars denote SEM. $^{***}P < 0.001$)

(Fig. 8a, blot 1, lane 3, red circle), indicating that $F3^{\Delta KPP}$ does not interact with $Tau^{RD\Delta K}$-His. Similarly, to confirm that $F3^{\Delta KPP}$ does not interact with other Tau variants, we co-expressed $F3^{\Delta KPP}$ with hTau40 in N2a cells and pulled down hTau40 with antibody DA9 that recognizes hTau40 but not $F3^{\Delta KPP}$. DA9 pulled down hTau40, but not $F3^{\Delta KPP}$ (Fig. 8a, blot 2, lane 3, red circle), suggesting that $F3^{\Delta KPP}$ does not interact with the full-length hTau40 either. These results show that the anti-aggregant $F3^{\Delta KPP}$ has a substantially different conformation than the pro-aggregant $F3^{\Delta K}$ which precludes a direct interaction.

To explain why $F3^{\Delta KPP}$ is able to inhibit aggregation without binding to hTau40 or $Tau^{RD\Delta K}$ one has to consider the ternary system of polycationic molecules like hTau40, $Tau^{RD\Delta K}$ or $F3^{\Delta KPP}$, and the polyanionic heparin. $F3^{\Delta KPP}$ competes with hTau40 or $Tau^{RD\Delta K}$ for the aggregation inducer heparin and in the process sequesters it. To test this hypothesis, we performed in vitro immunoprecipitation assays using recombinant proteins. We incubated the recombinant 50 μM hTau40 and 200 μM $F3^{\Delta KPP}$ (ratio 1:4) at 37 °C in the presence or absence of heparin for 48 h, and pulled down hTau40 using the DA9 antibody. DA9 pulled down both proteins hTau40 and $F3^{\Delta KPP}$ only when the two were incubated in the presence of heparin, but not in the absence of heparin (Fig. 8b, blots 1, 2, lanes 3). These results suggest either that hTau40, $F3^{\Delta KPP}$ and heparin form a complex that can be pulled down by the antibody DA9 directed against hTau40, or that heparin binds to both Tau proteins and to the magnetic beads that leads to pull down of the $F3^{\Delta KPP}$-Tau core. To confirm this, the recombinant proteins—after incubating at 37 °C for 48 h with or without heparin—were pulled down, this time without an antibody. Surprisingly, both hTau40 and $F3^{\Delta KPP}$ were pulled down when heparin was present in the solution, alone (Fig. 8c, blots 1, 2, lanes 2, red circles) or in combination (Fig. 8c, blot 3, lane 2, red circles). In the absence of heparin, none of the proteins was pulled down, alone (Fig. 8c, blots 1, 2, lanes 4) or in combination (Fig. 8c, blot 3, lane 4). These results confirm that heparin binds the recombinant proteins hTau40 and $F3^{\Delta KPP}$, and is able to pull down both of them by binding to the magnetic beads. Notably, heparin pulls down $F3^{\Delta KPP}$ almost completely compared to hTau40 as seen by the thick bands at $F3^{\Delta KPP}$ position in the pull-down lanes (compare in Fig. 8c lane 2 in blots 1, 2, red circles).

Furthermore, direct pull-down experiments without prior incubation of reaction mixtures at 37 °C led to the pull-down of $F3^{\Delta KPP}$ by heparin and not full-length Tau (Sup Fig. S2, red circle). These results show that $F3^{\Delta KPP}$ binds heparin with a higher affinity than full-length Tau, consistent with its higher specific positive charge. We therefore conclude that $F3^{\Delta KPP}$ inhibits the aggregation of $Tau^{RD\Delta K}$ or hTau40 by a competition and sequestration effect whereby $F3^{\Delta KPP}$ preferentially binds and engages the aggregation inducers like heparin. The effective reduction of aggregation inducers then results in the inhibition of $Tau^{RD\Delta K}$ or hTau40 aggregation.

Fig. 8 $F3^{\Delta KPP}$ does not interact directly with Tau40 or $Tau^{RD\Delta K}$ to prevent aggregation. N2a cells were co-transfected with $F3^{\Delta KPP}$ and $Tau^{RD\Delta K}$-His or hTau40 for 2 days. Antibody anti-His (blot A) and DA9 (epitope: aa. 112–129) (blot B) were used to immunoprecipitate $Tau^{RD\Delta K}$-His or hTau40 in the cell lysates respectively, using non-specific IgG as control (A, B, lane 2). **a** Anti-His pulled down $Tau^{RD\Delta K}$-His but not $F3^{\Delta KPP}$ (blot 1, lane 3). Similarly, DA9 pulled down hTau40 but not $F3^{\Delta KPP}$ (blot 2, lane 3), indicating that there is no direct interaction between $F3^{\Delta KPP}$ and hTau40. **b** Recombinant hTau40 (50 μM) and $F3^{\Delta KPP}$ (200 μM) were incubated at 37 °C for 48 h in the presence (blot 1) or absence (blot 2) of 12.5 μM heparin (M.W. 16 K) in BES buffer. Antibody DA9 (blots 1, 2, lane 3) was used to immunoprecipitate hTau40, using non-specific IgG as control (Ctrl-IgG, blots 1, 2, lane 2). Note that in the presence of heparin, DA9 pulls down both hTau40 and $F3^{\Delta KPP}$ (blot 1, lane 3). However, in the absence of heparin, DA9 pulls down only htau40 but not $F3^{\Delta KPP}$ (blot 2, lane 3), indicating an absence of a direct interaction between $F3^{\Delta KPP}$ and hTau40. **c** Heparin binds and pulls down $F3^{\Delta KPP}$ and hTau40 in the absence of antibody. Recombinant $F3^{\Delta KPP}$ and hTau40 at the same concentrations as described above were incubated at 37 °C for 48 h in the presence or absence of heparin (16 K) in BES buffer and Dynabeads Protein G added to the reaction mixtures afterwards. Note that hTau40 and $F3^{\Delta KPP}$ can be pulled down by heparin without requiring an antibody (blots 1, 2, 3, lane 2). In the absence of heparin, neither of the proteins is pulled down (blot 1, 2, 3, lane 4). Note the thick bands (red circle) corresponding to $F3^{\Delta KPP}$ in the pull-down lanes (blot 2, 3, lanes 2). This set of experiments shows (i) heparin is able to bind $F3^{\Delta KPP}$ and hTau40, (ii) heparin is able to bind the beads and thereby pull down both the proteins either individually or in combination, and (iii) the affinity is higher for $F3^{\Delta KPP}$ than hTau40. Hence, a direct interaction between $F3^{\Delta KPP}$ and hTau40 is absent, but the two interact indirectly via an aggregation inducer like heparin

Discussion

Tau aggregation characterizes Tauopathies including AD [26]. Numerous publications have reported that Tau aggregation causes or accompanies a neurotoxic process, though the precise nature of this remains a matter of debate [2]. Accordingly, suppressing Tau aggregation has long been proposed to be a therapeutic approach for AD and other Tauopathies. The development of low molecular weight inhibitors of Tau aggregation has been challenging because of Tau's variable conformations and because protein-protein interaction interfaces are generally flat and large, contrary to the deep cavities that small molecules can bind to [27]. During the past decade, several types of low MW compounds have been shown to inhibit Tau aggregation in vitro and in vivo [24, 28–31]. Methylene blue and its derivatives even entered clinical trials, although finally failed at phase III [32]. The caveat is that compounds may stabilize rather than disrupt the low-n oligomers (likely the more toxic species), if they form binding pockets for low MW compounds [33]. The increasing evidence that Tau oligomers are the most toxic species [34–36] may explain why

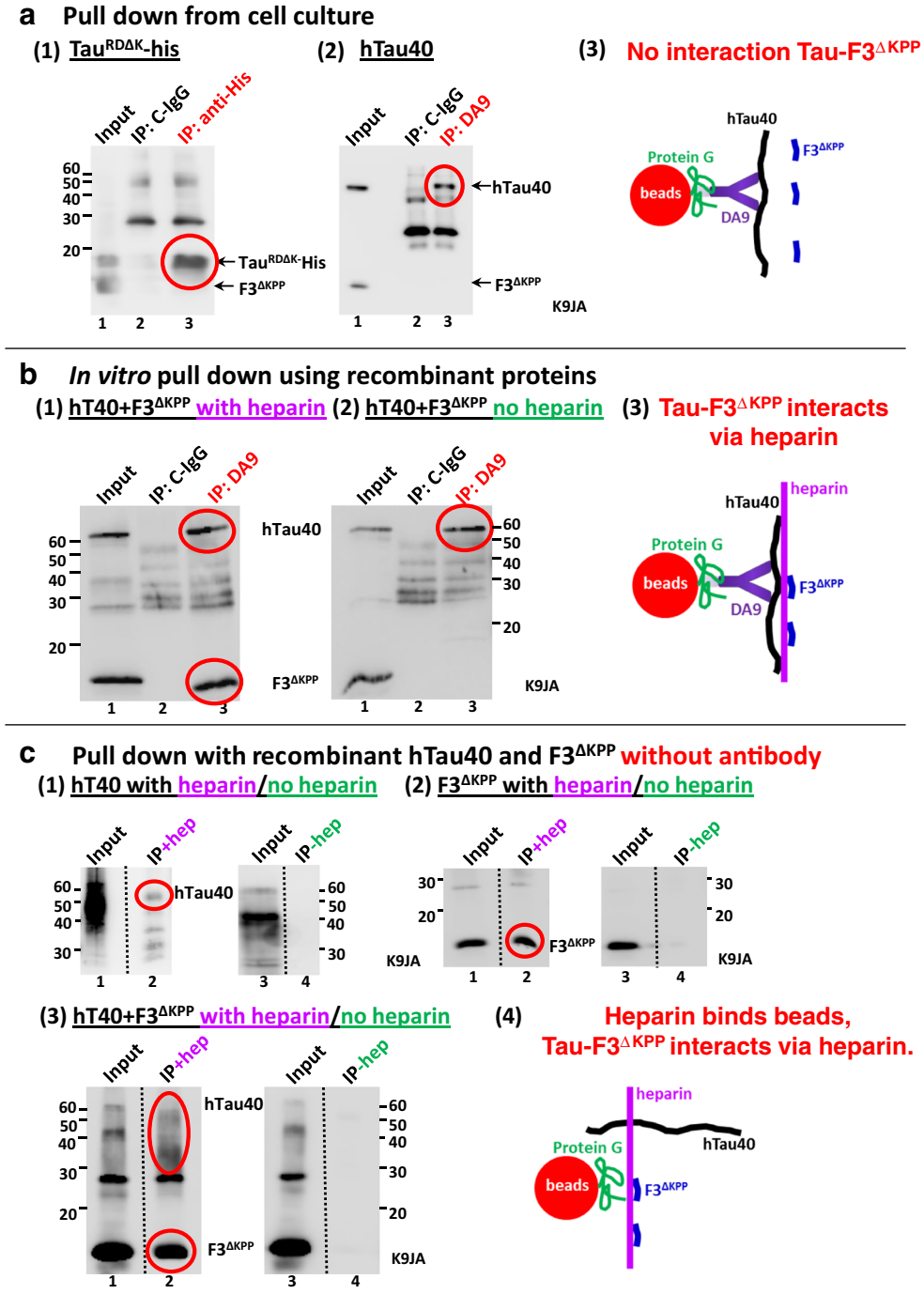

low MW Tau aggregation inhibitors have not yet succeeded in clinical trials. There is thus a need to search for alternative Tau aggregation inhibitors. Indeed, several groups are developing peptides targeting the two hexapeptide motifs of Tau that govern the Tau aggregation process [8, 37, 38]. The advantage to this approach is that the peptides occupy larger and more specific interaction interfaces between Tau molecules than low MW compounds, necessary to inhibit the overall aggregation process.

Here, we show that a β-structure breaker Tau fragment ($F3^{\Delta KPP}$) inhibits Tau aggregation and reduces Tau-induced cytotoxicity in vitro and in vivo (Figs. 2, 4, 5, 6 and 7). Surprisingly, $F3^{\Delta KPP}$ does not inhibit Tau aggregation via binding to Tau molecules, as no direct interaction of $F3^{\Delta KPP}$ with other Tau molecules was observed in vitro or in cultured cells (Fig. 8). Therefore, it is likely that the inhibition of aggregation is due to competition between $F3^{\Delta KPP}$ and Tau for aggregation inducers instead of a direct interaction

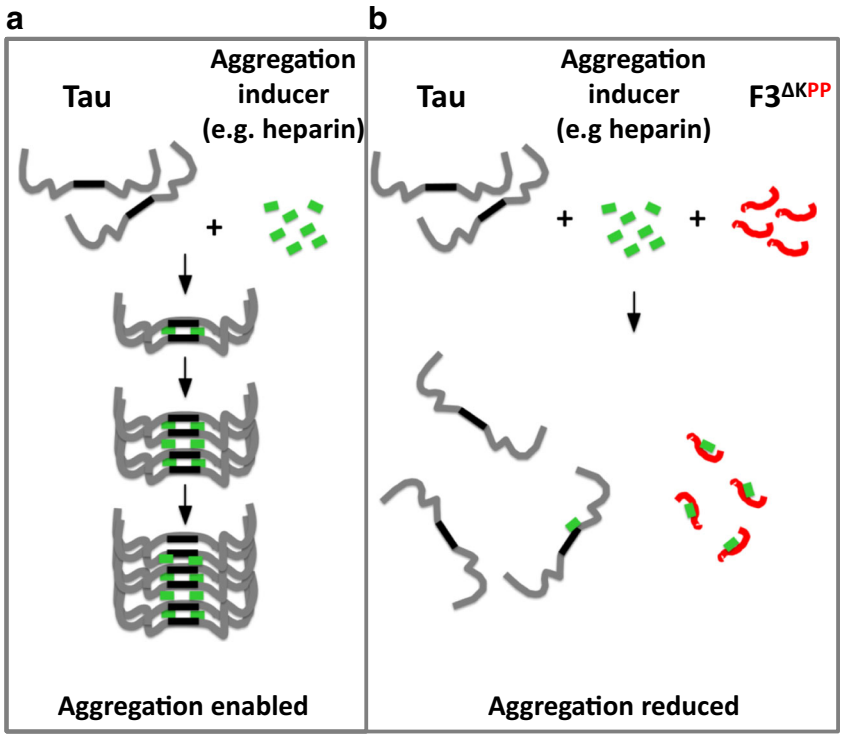

Fig. 9 Model of Tau aggregation and competition with anti-aggregant $F3^{\Delta KPP}$. Tau aggregation can be induced in vitro or in cells by cofactors such as heparin, RNA, or other polyanions (a). In such a scenario, $F3^{\Delta KPP}$ can compete with Tau molecules by preferentially binding and sequestering the aggregation inducers. This might prevent the formation of early oligomers (dimers, trimers etc.) (b). At low $F3^{\Delta KPP}$ levels, sufficient inducers are available so that the aggregation of Tau may not be disturbed. With increasing $F3^{\Delta KPP}$ levels, the inducers available for Tau are reduced and the aggregation of Tau is retarded

of $F3^{\Delta KPP}$ with Tau molecules. Tau contains multiple heparin binding sites as deducted from experiments using truncated Tau constructs, but the repeat region is indispensable for aggregation induced by heparin [39]. Despite being a derivative of the Tau repeat domain, $F3^{\Delta KPP}$ is incapable of aggregation due to proline substitutions in the two hexapeptide motifs that act as β-sheet breakers [5, 7]. Nevertheless, $F3^{\Delta KPP}$ is expected to have a similar affinity for polyanions like heparin. Indeed, in this study we show that $F3^{\Delta KPP}$ physically interacts with heparin. Notably, the $F3^{\Delta KPP}$ and heparin interaction is stronger than the full-length Tau and heparin interaction (Fig. 8c, blot 2, lane 2, compare with blot 1, lane 2, red circles). Thus, in a scenario where aggregation is induced by polyanions like heparin, $F3^{\Delta KPP}$ preferentially binds and sequesters such aggregation inducers and thereby, the aggregation process is halted.

The factors causing Tau aggregation in vivo remain a matter of debate. Post-translational modifications have been reported to contribute to Tau aggregation. However, it is unclear if they alone are sufficient to initiate Tau aggregation, given that no in vitro studies show the formation of abundant Tau fibrils by post-translationally modified Tau in the absence of cofactors [40]. Similarly, RNA molecules are capable of inducing Tau aggregation [41]. Recent studies show that Tau forms part of the stress granule pathway, which under pathological conditions leads to irreversible aggregation of RNA binding proteins [42, 43]. The interaction of Tau with ribosomes can inhibit protein synthesis and this interaction is based on RNA's and RNA binding proteins [44]. Besides, Tau may undergo reversible phase transition in cells in the presence of various cofactors [45, 46]. This phase transition from free soluble tau to liquid droplets might indeed represent early phases in the tau aggregation process. Other factors that could potentially induce Tau aggregation in vivo include sulphated glycosaminoglycans like heparin sulphate, chondroitin sulphate and dermatan sulphate. In the Alzheimer Disease brain, heparin sulphate coexists with Tau in tangle bearing neurons [47, 48] and neurons lacking neurofibrillary tangles may stain positive for hyperphosphorylated Tau [39]. Moreover, reports that sulphated glycosaminoglycans promote Tau phosphorylation by several kinases [49–51] and also prevent Tau binding to microtubules [52], suggest multiple effects favoring Tau aggregation.

Under physiological conditions, Tau prefers to bind to MT because of specific interactions, in addition to the electrostatic interactions of oppositely charged polymers [53]. Furthermore, this interaction of Tau with MT actually prevents interaction between the β-structure forming parts of Tau and thereby prevents self-assembly of Tau [54]. Under pathological conditions, the affinity of Tau to MT can be reduced by post-translational modifications (e.g., phosphorylation). As such, Tau may be induced to aggregate by inducers like RNA and/or heparin sulphate. Hence $F3^{\Delta KPP}$, unable to contribute to filamentous assembly due to absence of β-structure, can instead compete with other

Tau molecules for these aggregation inducers. Thus, when the concentration of $F3^{\Delta KPP}$ is low, the amount of the available inducers (e.g., heparin, RNA, or other cellular polyanions) may be sufficient to trigger the aggregation of other Tau molecules, but with increasing $F3^{\Delta KPP}$ levels the inducers available for other Tau molecules are reduced, resulting in the reduction of aggregated Tau (Fig. 9). In conclusion, we revealed that a β-structure breaker Tau fragment ($F3^{\Delta KPP}$) can inhibit Tau aggregation and Tau-induced cytotoxicity. This β-structure breaker Tau fragment may have potential as a therapeutic approach for Tauopathies.

Acknowledgements The authors thank Dr. J. Biernat (DZNE Bonn) for the generation of inducible N2a cell models and Tau constructs, S. Hübschmann for excellent technical assistance, Christoph Klatt for EM handling and Dr. Daniele Bano (DZNE, Bonn) for his support. We thank Dr. P. Seubert (Elan Pharma, South San Francisco, CA, USA) for antibody 12E8 and Dr. P. Davies (Albert Einstein College, New York) for PHF1 antibody. This work was supported by DZNE, MPG, K-Hardt Foundation.

Author Contributions GJP, YW conceived and designed the experiments. GJP performed the worm work and the in vitro IP assays. YW performed the in vitro and the cell culture work. BC performed the worm work. SK performed the in vitro work, AFM, and EM. RRC performed the microtubule assembly assay. GJP, YW analyzed the data and wrote the manuscript. EM and E-MM supervised the study and took part in data analysis and writing of the manuscript. All authors revised the article critically for intellectual content and have read and approved the final version of the manuscript.

Funding Information Open access funding provided by Center of Advanced European Studies and Research (CAESAR).

Compliance with Ethical Standards

Competing Interests The authors declare that they have no conflict of interest.

Abbreviations 2N4R-Tau, isoform 2, largest isoform of human Tau in CNS (441 residues, 2 inserts +4 repeats), accession: NP_005901.2, amino acid numbering based on full-length human 2N4R isoform; 1N4R-Tau, human Tau isoform 5 in CNS (412 residues, 1 insert +4 repeats), accession: NP_001116539.1, amino acid numbering based on full-length human 2N4R isoform; AFM, atomic force microscopy; ANOVA, analysis of variance; EM, electron microscopy; $F3^{\Delta KPP}$, Tau repeat domain fragment with ΔK mutation and two proline substitutions in the hexapeptide motifs (258–360 residues); MAPT, microtubule-associated protein Tau; non-Tg, non-transgenic; T^{VM}, worms expressing mutant V337 M human 1N4R-Tau; T^{VM};$F3^{\Delta KPP}$-hi, double transgenic worm expressing T^{V337M}, and $F3^{\Delta KPP}$ at higher levels; T^{VM};$F3^{\Delta KPP}$-lo, double transgenic worm expressing T^{V337M}, and $F3^{\Delta KPP}$ at lower levels; $Tau^{RD\Delta K}$, Tau repeat domain with ΔK280 mutation (244–372 residues, 4 repeat); ThS, thioflavine S; VNC, ventral nerve cord

Open Access This article is distributed under the terms of the Creative Commons Attribution 4.0 International License (http://creativecommons.org/licenses/by/4.0/), which permits unrestricted use, distribution, and reproduction in any medium, provided you give appropriate credit to the original author(s) and the source, provide a link to the Creative Commons license, and indicate if changes were made.

References

1. Braak H, Braak E (1991) Demonstration of amyloid deposits and neurofibrillary changes in whole brain sections. Brain Pathol 1:213–216
2. WANG Y, MANDELKOW E (2016) Tau in physiology and pathology. Nat Rev Neurosci 17:5–21
3. Devos SL, Goncharoff DK, Chen G, Kebodeaux CS, Yamada K, Stewart FR, Schuler DR, Maloney SE et al (2013) Antisense reduction of tau in adult mice protects against seizures. J Neurosci 33: 12887–12897
4. ROBERSON ED, SCEARCE-LEVIE K, PALOP JJ, YAN F, CHENG IH, WU T, GERSTEIN H, YU GQ et al (2007) Reducing endogenous tau ameliorates amyloid beta-induced deficits in an Alzheimer's disease mouse model. Science 316:750–754
5. VON BERGEN M, FRIEDHOFF P, BIERNAT J, HEBERLE J, MANDELKOW EM, MANDELKOW E (2000) Assembly of tau protein into Alzheimer paired helical filaments depends on a local sequence motif ((306)VQIVYK(311)) forming beta structure. Proc Natl Acad Sci U S A 97:5129–5134
6. VON BERGEN M, BARGHORN S, LI L, MARX A, BIERNAT J, MANDELKOW EM, MANDELKOW E (2001) Mutations of tau protein in frontotemporal dementia promote aggregation of paired helical filaments by enhancing local beta-structure. J Biol Chem 276:48165–48174
7. SYDOW A, VAN DER JEUGD A, ZHENG F, AHMED T, BALSCHUN D, PETROVA O, DREXLER D, ZHOU L et al (2011) Tau-induced defects in synaptic plasticity, learning, and memory are reversible in transgenic mice after switching off the toxic Tau mutant. J Neurosci 31:2511–2525
8. SIEVERS SA, KARANICOLAS J, CHANG HW, ZHAO A, JIANG L, ZIRAFI O, STEVENS JT, MUNCH J et al (2011) Structure-based design of non-natural amino-acid inhibitors of amyloid fibril formation. Nature 475:96–100
9. KIM YS, LIM D, KIM JY, KANG SJ, KIM YH, IM H (2009) Beta-sheet-breaking peptides inhibit the fibrillation of human alpha-synuclein. Biochem Biophys Res Commun 387:682–687
10. SOTO C, KASCSAK RJ, SABORIO GP, AUCOUTURIER P, WISNIEWSKI T, PRELLI F, KASCSAK R, MENDEZ E et al (2000) Reversion of prion protein conformational changes by synthetic beta-sheet breaker peptides. Lancet 355:192–197
11. Di L (2015) Strategic approaches to optimizing peptide ADME properties. AAPS J 17:134–143
12. NALDINI L (2015) Gene therapy returns to Centre stage. Nature 526:351–360
13. KHLISTUNOVA I, BIERNAT J, WANG Y, PICKHARDT M, VON BERGEN M, GAZOVA Z, MANDELKOW E, MANDELKOW EM (2006) Inducible expression of tau repeat domain in cell models of tauopathy: aggregation is toxic to cells but can be reversed by inhibitor drugs. J Biol Chem 281:1205–1214
14. MOCANU MM, NISSEN A, ECKERMANN K, KHLISTUNOVA I, BIERNAT J, DREXLER D, PETROVA O, SCHONIG K et al (2008) The potential for beta-structure in the repeat domain of tau protein determines aggregation, synaptic decay, neuronal loss, and coassembly with endogenous Tau in inducible mouse models of tauopathy. J Neurosci 28:737–748
15. VAN DER JEUGD A, HOCHGRAFE K, AHMED T, DECKER JM, SYDOW A, HOFMANN A, WU D, MESSING L et al (2012) Cognitive defects are reversible in inducible mice expressing pro-aggregant full-length human Tau. Acta Neuropathol 123:787–805
16. Barghorn S, Biernat J, Mandelkow E (2005) Purification of recombinant tau protein and preparation of Alzheimer-paired helical filaments in vitro. Methods Mol Biol 299:35–51
17. WANG YP, BIERNAT J, PICKHARDT M, MANDELKOW E, MANDELKOW EM (2007) Stepwise proteolysis liberates

tau fragments that nucleate the Alzheimer-like aggregation of full-length tau in a neuronal cell model. Proc Natl Acad Sci U S A 104:10252–10257
18. WANG Y, MARTINEZ-VICENTE M, KRUGER U, KAUSHIK S, WONG E, MANDELKOW EM, CUERVO AM, MANDELKOW E (2009) Tau fragmentation, aggregation and clearance: the dual role of lysosomal processing. Hum Mol Genet 18:4153–4170
19. Brenner S (1974) The genetics of Caenorhabditis elegans. Genetics 77:71–94
20. Gao S, Zhen M (2011) Action potentials drive body wall muscle contractions in Caenorhabditis elegans. Proc Natl Acad Sci U S A 108:2557–2562
21. PICKHARDT M, BIERNAT J, HUBSCHMANN S, DENNISSEN FJA, TIMM T, AHO A, MANDELKOW EM, MANDELKOW E (2017) Time course of Tau toxicity and pharmacologic prevention in a cell model of Tauopathy. Neurobiol Aging 57:47–63
22. KRAEMER BC, ZHANG B, LEVERENZ JB, THOMAS JH, TROJANOWSKI JQ, SCHELLENBERG GD (2003) Neurodegeneration and defective neurotransmission in a Caenorhabditis elegans model of tauopathy. Proc Natl Acad Sci U S A 100:9980–9985
23. LUNDQUIST EA, REDDIEN PW, HARTWIEG E, HORVITZ HR, BARGMANN CI (2001) Three C. elegans Rac proteins and several alternative Rac regulators control axon guidance, cell migration and apoptotic cell phagocytosis. Development 128: 4475–4488
24. Fatouros C, Pir GJ, Biernat J, Koushika SP, Mandelkow E, Mandelkow EM, Schmidt E, Baumeister R (2012) Inhibition of tau aggregation in a novel Caenorhabditis elegans model of tauopathy mitigates proteotoxicity. Hum Mol Genet 21:3587–3603
25. THIES E, MANDELKOW EM (2007) Missorting of tau in neurons causes degeneration of synapses that can be rescued by the kinase MARK2/Par-1. J Neurosci 27:2896–2907
26. Goedert M, Eisenberg DS, Crowther RA (2017) Propagation of Tau aggregates and neurodegeneration. Annu Rev Neurosci 40:189–210
27. Arkin MR, Tang Y, Wells JA (2014) Small-molecule inhibitors of protein-protein interactions: Progressing toward the reality. Chem Biol 21:1102–1114
28. Bulic B, Pickhardt M, Mandelkow E (2013) Progress and developments in tau aggregation inhibitors for Alzheimer disease. J Med Chem 56:4135–4155
29. MELIS V, MAGBAGBEOLU M, RICKARD JE, HORSLEY D, DAVIDSON K, HARRINGTON KA, GOATMAN K, GOATMAN EA et al (2015) Effects of oxidized and reduced forms of methylthioninium in two transgenic mouse tauopathy models. Behav Pharmacol 26:353–368
30. PICKHARDT M, NEUMANN T, SCHWIZER D, CALLAWAY K, VENDRUSCOLO M, SCHENK D, ST GEORGE-HYSLOP P, MANDELKOW EM et al (2015) Identification of small molecule inhibitors of Tau aggregation by targeting monomeric Tau as a potential therapeutic approach for Tauopathies. Curr Alzheimer Res 12:814–828
31. SCHIRMER RH, ADLER H, PICKHARDT M, MANDELKOW E (2011) Lest we forget you–methylene blue. Neurobiol Aging 32(2325):e7–e16
32. Gauthier S, Feldman HH, Schneider LS, Wilcock GK, Frisoni GB, Hardlund JH, Moebius HJ, Bentham P et al (2016) Efficacy and safety of tau-aggregation inhibitor therapy in patients with mild or moderate Alzheimer's disease: a randomised, controlled, double-blind, parallel-arm, phase 3 trial. Lancet 388:2873–2884
33. Akoury E, Gajda M, Pickhardt M, Biernat J, Soraya P, Griesinger C, Mandelkow E, Zweckstetter M (2013) Inhibition of tau filament formation by conformational modulation. J Am Chem Soc 135: 2853–2862
34. KANIYAPPAN S, CHANDUPATLA RR, MANDELKOW EM, MANDELKOW E (2017) Extracellular low-n oligomers of tau cause selective synaptotoxicity without affecting cell viability. Alzheimers Dement 13:1270–1291
35. LASAGNA-REEVES CA, CASTILLO-CARRANZA DL, SENGUPTA U, CLOS AL, JACKSON GR, KAYED R (2011) Tau oligomers impair memory and induce synaptic and mitochondrial dysfunction in wild-type mice. Mol Neurodegener 6:39
36. TAI HC, WANG BY, SERRANO-POZO A, FROSCH MP, SPIRES-JONES TL, HYMAN BT (2014) Frequent and symmetric deposition of misfolded tau oligomers within presynaptic and postsynaptic terminals in Alzheimer's disease. Acta Neuropathol Commun 2:146
37. Dammers C, Yolcu D, Kukuk L, Willbold D, Pickhardt M, Mandelkow E, Horn AH, Sticht H et al (2016) Selection and characterization of tau binding -enantiomeric peptides with potential for therapy of Alzheimer disease. PLoS One 11:e0167432
38. PLUMLEY JA, ALI-TORRES J, POHL G, DANNENBERG JJ (2014) Capping amyloid beta-sheets of the tau-amyloid structure VQIVYK with hexapeptides designed to arrest growth. An ONIOM and density functional theory study. J Phys Chem B 118: 3326–3334
39. Goedert M, Jakes R, Spillantini MG, Hasegawa M, Smith MJ, Crowther RA (1996) Assembly of microtubule-associated protein tau into Alzheimer-like filaments induced by sulphated glycosaminoglycans. Nature 383:550–553
40. TEPPER K, BIERNAT J, KUMAR S, WEGMANN S, TIMM T, HUBSCHMANN S, REDECKE L, MANDELKOW EM et al (2014) Oligomer formation of tau protein hyperphosphorylated in cells. J Biol Chem 289:34389–34407
41. Kampers T, Friedhoff P, Biernat J, Mandelkow EM, Mandelkow E (1996) RNA stimulates aggregation of microtubule-associated protein tau into Alzheimer-like paired helical filaments. FEBS Lett 399:344–349
42. Apicco DJ, Ash PEA, Maziuk B, Leblang C, Medalla M, Al Abdullatif A, Ferragud A, Botelho E et al (2018) Reducing the RNA binding protein TIA1 protects against tau-mediated neurodegeneration in vivo. Nat Neurosci 21:72–80
43. VANDERWEYDE T, YU H, VARNUM M, LIU-YESUCEVITZ L, CITRO A, IKEZU T, DUFF K, WOLOZIN B (2012) Contrasting pathology of the stress granule proteins TIA-1 and G3BP in tauopathies. J Neurosci 32:8270–8283
44. MEIER S, BELL M, LYONS DN, Rodriguez-Rivera J, Ingram A, Fontaine SN, Mechas E, Chen J et al (2016) Pathological Tau promotes neuronal damage by impairing ribosomal function and decreasing protein synthesis. J Neurosci 36:1001–1007
45. WEGMANN S, EFTEKHARZADEH B, TEPPER K, ZOLTOWSKA KM, BENNETT RE, DUJARDIN S, LASKOWSKI PR, MACKENZIE D et al (2018) Tau protein liquid-liquid phase separation can initiate tau aggregation. EMBO J 37:e98049
46. ZHANG X, LIN Y, ESCHMANN NA, ZHOU H, RAUCH JN, HERNANDEZ I, GUZMAN E, KOSIK KS et al (2017) RNA stores tau reversibly in complex coacervates. PLoS Biol 15: e2002183
47. PERRY G, SIEDLAK SL, RICHEY P, KAWAI M, CRAS P, KALARIA RN, GALLOWAY PG, SCARDINA JM et al (1991) Association of heparan sulfate proteoglycan with the neurofibrillary tangles of Alzheimer's disease. J Neurosci 11:3679–3683
48. SNOW AD, MAR H, NOCHLIN D, SEKIGUCHI RT, KIMATA K, KOIKE Y, WIGHT TN (1990) Early accumulation of heparan sulfate in neurons and in the beta-amyloid protein-containing lesions of Alzheimer's disease and Down's syndrome. Am J Pathol 137:1253–1270
49. Brandt R, Lee G, Teplow DB, Shalloway D, Abdel-Ghany M (1994) Differential effect of phosphorylation and substrate

modulation on tau's ability to promote microtubule growth and nucleation. J Biol Chem 269:11776–11782
50. MAWAL-DEWAN M, SEN PC, ABDEL-GHANY M, SHALLOWAY D, RACKER E (1992) Phosphorylation of tau protein by purified p34cdc28 and a related protein kinase from neurofilaments. J Biol Chem 267:19705–19709
51. YANG SD, YU JS, SHIAH SG, HUANG JJ (1994) Protein kinase FA/glycogen synthase kinase-3 alpha after heparin potentiation phosphorylates tau on sites abnormally phosphorylated in Alzheimer's disease brain. J Neurochem 63: 1416–1425
52. Biernat J, Gustke N, Drewes G, Mandelkow EM, Mandelkow E (1993) Phosphorylation of Ser262 strongly reduces binding of tau to microtubules: distinction between PHF-like immunoreactivity and microtubule binding. Neuron 11:153–163
53. Kadavath H, Hofele RV, Biernat J, Kumar S, Tepper K, Urlaub H, Mandelkow E, Zweckstetter M (2015) Tau stabilizes microtubules by binding at the interface between tubulin heterodimers. Proc Natl Acad Sci U S A 112:7501–7506
54. Ackmann M, Wiech H, Mandelkow E (2000) Nonsaturable binding indicates clustering of tau on the microtubule surface in a paired helical filament-like conformation. J Biol Chem 275:30335–30343